Automatic Generation and Detection of Visually Faultless Facial Morphs

Andrey Makrushin, Tom Neubert and Jana Dittmann
Otto-von-Guericke University of Magdeburg, Universitaetsplatz 2, Magdeburg, Germany
andrey.makrushin@ovgu.de, {tom.neubert, jana.dittmann}@iti.cs.uni-magdeburg.de

Keywords: Face Morph, Morphing Attack, Automatic Face Recognition, Morph Detection, Digital Image Forensics.

Abstract: This paper introduces an approach to automatic generation of visually faultless facial morphs along with a proposal on how such morphs can be automatically detected. It is endeavored that the created morphs cannot be recognized as such with the naked eye and a reference automatic face recognition (AFR) system produces high similarity scores while matching a morph against faces of persons who participated in morphing. Automatic generation of morphs allows for creating abundant experimental data, which is essential (i) for evaluating the performance of AFR systems to reject morphs and (ii) for training forensic systems to detect morphs. Our first experiment shows that human performance to distinguish between morphed and genuine face images is close to random guessing. In our second experiment, the reference AFR system has verified 11.78% of morphs against any of genuine images at the decision threshold of 1% false acceptance rate. These results indicate that facial morphing is a serious threat to access control systems aided by AFR and establish the need for morph detection approaches. Our third experiment shows that the distribution of Benford features extracted from quantized DCT coefficients of JPEG-compressed morphs is substantially different from that of genuine images enabling the automatic detection of morphs.

1 INTRODUCTION

Face as a biometric modality is a widely accepted means of personal identity verification. For many years, a printed facial image has been an important part of identification documents. Recently, printed face images have been supplemented by digital face images stored on a chip integrated in the document. On the one hand, issuing machine-readable documents with digital photographs opens up new horizons for applying Automatic Face Recognition (AFR) systems to identity verification which saves expensive manpower. On the other hand, the risk of criminal intent to overcome AFR systems arises.

One of the possible attacks is brought to the forefront by Ferrara et al. (Ferrara, 2014). This so-called morphing attack is based on blending digital face images of a criminal and his accomplice resulting in a morphed face image (morph), which is visually similar to both faces: the accomplice's face and the criminal's face. As a result, two persons can share one document.

In order to confirm the severity of this attack, Ferrara et al. (Ferrara, 2016) evaluated the human performance to match faces in original and morphed images as well as the performance of three commercial AFR systems to reject morphs. The conclusions raise a major concern because, in many cases, testees said that genuine and morphed face images depict the same person and the experts were not better in performing this task than laymen. Even worse results came from AFR systems. The Morph Acceptance Rate (MAR) at the decision thresholds of 1% and 0.1% False Acceptance Rate (FAR) is confirmed to be very high, indicating that the tested systems are not able to distinguish between morphed and genuine face images.

All in all, the systematic analysis of the morphing attack has to be performed including the study on morphing generation approaches as well as the development of approaches to automatic morph detection.

The morphs in (Ferrara, 2016) include a manual retouch, which makes morph generation very time consuming. There have only been 80 morphs generated resulting in 160 morph verification attempts for computing MAR. To the best of our knowledge, there are currently no large publicly available datasets of facial morphs. Therefore, we propose an algorithm for automatic generation of morphs enabling fast creation of thousands of

Makrushin A., Neubert T. and Dittmann J.
Automatic Generation and Detection of Visually Faultless Facial Morphs.
DOI: 10.5220/0006131100390050
In *Proceedings of the 12th International Joint Conference on Computer Vision, Imaging and Computer Graphics Theory and Applications (VISIGRAPP 2017)*, pages 39-50
ISBN: 978-989-758-227-1

realistic morphs. Possessing a large database of multifarious morphs allows (i) for statistically significant estimation of MAR, thus establishing the resistance of AFR systems against the morphing attack and (ii) for training and evaluation of forensic morph detection algorithms.

For our experiments, we generated 3940 halfway facial morphs from the Utrecht ECVP face dataset (http://pics.psych.stir.ac.uk/2D_face_sets.htm) and 500 morphs from FEI Face Database (http://fei.edu.br/~cet/facedatabase.html).

The visual quality of our morphs is proven in the experiment on human perception of morphs. In contrast to (Ferrara, 2016), in our experiment, a testee decides for each single image whether it is a morph or not. Human failure to reveal a morph indicates its visual faultlessness. The MAR of humans is 44.60% while the False Rejection Rate (FRR) is 43.64%.

Next, we tested our morphs with the Luxand Face SDK 6.1 (https://www.luxand.com/facesdk/) which is taken as a reference COTS AFR system. At the thresholds of 1% and 0.1% FAR, the MAR yields 60.59% and 53.77% correspondingly. Nonetheless, only 11.78% of morphs have been verified against any of genuine images at 1% FAR and 3.21% of morphs at 0.1% FAR.

The poor performance of AFR systems to reject morphs motivates us to work on automatic morph detection. Our detector is based on Benford features calculated from quantized Discrete Cosine Transformation (DCT) coefficients of JPEG-compressed images. Classification of feature vectors is performed using a linear Support Vector Machine (SVM). We state and experimentally show that the distributions of Benford features are substantially different for morphed and genuine images. The MAR of our morph detector does not exceed 13%.
Our contributions can be summarized as follows:

- we introduce a splicing-based approach to automatic generation of visually faultless facial morphs (Section 4.1) and evaluate the quality of the morphs experimentally in a human test (Section 5.4) and with a COTS AFR system (Section 5.5);
- we introduce an automatic morph detection approach based on Benford features and linear SVM classifier (Section 4.2) and evaluate its classification performance (Section 5.6).

Hereafter, the paper is organized as follows. Related work is summarized in Section 2 including recent advances in automation of facial morphing and standard approaches of digital image forensics. Section 3 encompasses the theoretical background of facial morphing and tampering detection based on JPEG compression artifacts. In Section 4, our approaches to automatic morph generation and detection are introduced. Our experiments are presented in Section 5. Section 6 concludes the paper with the results and future work.

2 RELATED WORK

2.1 Facial Morphing

Morphing or “Metamorphosis” is a well-studied topic in computer graphics. A brief survey on morphing approaches is given in (Wolberg, 1998). Generally, morphing can be seen as a combination of image warping and a cross-dissolve of image elements. Wolberg in (Wolberg, 1990) summarizes the fundamentals of image warping focusing on the mesh warping technique. The most frequently referenced morphing technique is, however, feature-based warping introduced in (Beier, 1992). The authors suggest locating pairs of corresponding line segments and designing the mapping function for each point based on the distance to each line. Further techniques suggest locating pairs of corresponding key points and applying the same mapping functions to local neighborhoods around these points (Arad, 1994; Lee, 1996).

Early morphing approaches, mostly applied in the film industry as a computer animation tool, have always required human assistance to specify image features. Modern morphing approaches evolve towards automatic establishing of structural similarity between objects in source and target images (Liao, 2014).

A human face seems to be a favorite object for morphing, because it is very intuitive and impressive to visualize aging or a metamorphosis of one human to another.

Blanz and Vetter (Blanz, 1999) introduce a technique for face and face pose morphing comprised of fitting the morphable 3D model to a 2D face image and modifying the resulting individual 3D face towards another individual or another pose exploiting principal component analysis. However, this approach requires manual assistance to obtain an accurate alignment between the morphable model and a face in the image.

The efforts towards automatic generation of facial morphs start with locating facial features in a fully automated way. Cootes et al. (Cootes, 2000) propose the concept of Active Shape Models to

locate key points using local template matching employing constraints of the shape models. This concept is effectively used to locate facial landmarks and to modify face appearance easily, representing another way of face morphing. ASM is applied in (Zanella, 2009) to face images in a frontal view to perform morphing automatically. A comprehensive survey on locating facial landmarks is presented in (Celiktutan, 2013).

In spite of recent advances in facial morphing, the automatic generation of visually faultless facial morphs is still a very challenging task. The diversity of facial images including different poses, skin colors, hair styles and illumination conditions drastically influences the appearance of automatically generated morphs making them look less realistic. One way to visually improve morphs is retouching photographs to remove unrealistic hair and spurious shadows caused by cross-dissolving of images. An automatic interpolation of hair for portrait morphing is addressed in (Weng, 2013). Another way to achieve a realistic appearance is to cut facial regions, warp them, blend them to a mutual face, and seamlessly stitch it back into one of the input images. We refer to the result of this strategy as a *splicing morph*. A splicing morph is taken as an opposite of a *complete morph* that could be seen as a result of warping and blending of complete facial images including hair, torso and background. We focus on generation of the former, because the visual inaccuracies created by splicing are easier to conceal. A relatively simple and straight-forward way to achieve seamless stitching during generation of splicing morphs is automatic selection of similar input images as suggested in (Bitouk, 2008) for swapping faces or in (Vyas, 2015) for morphing.

2.2 Detection of Face Morphs

Since facial morphing can be seen as a special case of tampering with image content, well-established approaches to tampering detection from the field of digital image forensics can be adopted. Indeed, a morphing process along with a subsequent retouch, on the one hand, creates specific artifacts in the image and, on the other hand, destroys a camera-specific fingerprint. Standard techniques of digital image forensics are summarized in (Farid, 2009).

Notice that different morphing approaches create different inconsistencies. For instance, the aforementioned splicing morphs represent a special case of image insertion or image splicing also referred to as a cut-and-paste attack (Piva, 2013).

In (Schetinger, 2016) the "indirect arms race" between image tampering and image forensics is discussed. The authors assign image morphing to the group "Image Enhancement/Tweaking" and state: "Even though image insertion and manipulation can create visually convincing results, they should not pose a problem for modern forensic techniques."

Dealing with morphed images created by an attacker, a forensic expert is limited to so-called "blind" approaches, implying that no other information except for the probe image is presented for analysis. The most complete bibliography on blind tampering detection is gathered in (Mahdian, 2010). Image splicing detection is a substantial part in this review.

There are three basic clues to detect splicing independently from the image content. These are: noise distribution (Lyu, 2014), demosaicing inconsistencies (Dirik, 2009; Ferrara, 2012) and compression artifacts (Lukas, 2003; Bianchi, 2012; Milani, 2014).

Camera Noise is also referred to as Photo Response Non-Uniformity (PRNU) of the camera sensor and considered to be unique for each camera (Fridrich, 2009). However, splicing detection from PRNU is traditionally performed in the presence of camera reference images. An alternative approach to exposing spliced regions by means of noise estimation is presented in (Lyu, 2014).

Demosaicing, also referred to as Color Filter Array (CFA) interpolation, arises in color images because standard sensors capture only a single color value at each pixel location and the missing colors are interpolated from the adjacent pixels. Tampering detection (Dirik, 2009) as well as fine-grained splicing detection (Ferrara, 2012) by analyzing demosaicing inconsistencies has been proven an effective technique so long as fragile CFA traces have not been destroyed by legitimate image editing. It is mentioned in (Schetinger, 2016) that even a simple median or Gaussian filter is able to remove CFA traces. Nonetheless, CFA analysis is effective to distinguish native and non-native images, and therefore can be applied to detection of splicing morphs generated from raw images. Image morphing detection by analyzing CFA traces is addressed in (Ghatol, 2013).

Compression Artifacts arise in images after lossy compression performed by a camera or by a photographer after editing a raw image. After tampering with image content, images are often re-compressed. The vast majority of tampering detection approaches deal with JPEG as the most common compression standard. In order to detect

double JPEG compression, most of the algorithms rely on the analysis of the histogram of DCT coefficients (Piva, 2013). A recent study utilizing this idea (Bianchi, 2012) performs block-grained localization of tampered regions in the presence of aligned and non-aligned double JPEG compression. Milani et al. (Milani, 2014) advocate the idea of using first digit features also referred to as Benford features to identify a level of compression.

Analysis of JPEG compression inconsistency is especially promising for detection of splicing morphs. Since the original images used for morph generation are often JPEG-compressed, a morphed image contains the original background blocks with compression artifacts and synthetic face blocks with destroyed compression artifacts due to interpolation and cross-dissolve. Hence, the compressed splicing morphs should contain blocks with different levels of compression.

In (Schetinger, 2016), CFA and double JPEG compression artifacts are asserted to be plausible traces for morphing detection and noise to be an identifiable trace.

The most recent effort to withstand the attack from (Ferrara, 2014) is reported in (Ramachandra, 2016) introducing a morph detection approach based on binarized statistical image features used in conjunction with a linear SVM.

3 GENERAL DEFINITIONS OF MORPHING AND BENFORD FEATURES

3.1 Facial Morphing

Morphing is defined as a process of fluid transformation of one digital image (source) into another (target). Generation of intermediate images is realized by image warping supplemented by color interpolation. Warping is a geometric transformation applied to one or both images aiming at alignment between important image features. We rely on the mesh warping technique setting mesh elements to triangles. Color interpolation can be understood as alpha-blending of intensity values of both images for each color layer separately. The parameter alpha defines the proportion of pixel intensity values obtained from source and target images.

In the case of facial morphing, the features are defined by key points depicting eyes, nose, mouth and face contour. The warping functions are defined for the triangles built by the triplets of the key points. Mapping of triangles is known to be the standard affine transformation whose coefficients can be easily and efficiently found. Any kind of triangulation is theoretically possible. Practically, it is shown that Delaunay triangulation yields convincing results (Wu, 2011). We further use the term facial landmarks to refer to the key points.

There are two ways to warp images: forward and reverse mapping. Forward mapping starts with a pixel within the source image and transfers it into the corresponding location in the destination image. Reverse mapping starts with a pixel within the destination image and looks for its color in the source image at the corresponding location. Forward mapping might lead to unpainted pixels in the destination image. Contrary to this, reverse mapping ensures that every pixel in the destination image obtains a value.

For the source (I^s) and target (I^t) input face images, the procedure of generation of intermediate frames I^α can be formally described as follows:

1. define α from the interval [0,1]
2. find facial landmarks $L^s = \{l^s_j, j=1..n\}$ and $L^t = \{l^t_j, j=1..n\}$
3. create blended landmarks $L^m = \{l^m_j: l^m_j = (1-\alpha)\cdot l^s_j + \alpha\cdot l^t_j, j=1..n\}$
4. create set of triangles $T = \{t_i: t_i=(a,b,c), a,b,c \in L^m, i=1..k\}$
5. initialize warped images I^{sw} and I^{tw}
6. for each t_i
   I_i denotes the set of pixels in I enclosed in the triangle t_i (e.g. I^s_i, I^t_i, I^{sw}_i and I^{tw}_i)
   6.1 create mapping functions:
   $f^s_i: Z^{+2} \rightarrow Z^{+2}$ and $f^t_i: Z^{+2} \rightarrow Z^{+2}$
   6.2 apply these:
   $I^{sw}_i = f^s_i(I^s_i)$ and $I^{tw}_i = f^t_i(I^t_i)$
7. $I^{sw} = \{I^{sw}_i, i=1..k\}$ and $I^{tw} = \{I^{tw}_i, i=1..k\}$
8. $I^\alpha = (1-\alpha)\cdot I^{sw} + \alpha\cdot I^{tw}$

where n is the number of landmarks and k is the number of triangles.

3.2 Morph Detection by Analyzing JPEG Compression Artifacts

Facing the diversity of morphing techniques, the creation of a general morph detection algorithm is extremely challenging. Quite to the contrary, the algorithms for detection of particular types of facial morphs can be developed with far less effort. However, detection of morphs requires the thorough understanding of the morph generation process and possible image artifacts resulting from it.

We believe that splicing morphs can be efficiently detected by analyzing JPEG compression artifacts. Our hypothesis is that a morphed image contains blocks from the original image that have already undergone a JPEG compression as well as synthetic blocks generated by the morphing process. These blocks are uncompressed. If the morphed image undergoes JPEG compression, the original blocks become double-compressed and the synthetic blocks are single-compressed.

In order to comprehend the features that we use for morph detection, let us look at the process of JPEG compression which is comprised of three basic steps: DCT, quantization and entropy coding.

Firstly, the color space of an image is transformed from RGB to YCbCr. Notice that the color levels are processed independently. Each layer is divided into non-overlapping blocks of 8x8 pixels and the DCT is applied to these blocks resulting in 64 DCT coefficients. Each coefficient represents the contribution (amplitude) of a certain cosine function to the linear combination of cosine functions oscillating at different frequencies. This linear combination represents the original signal. In other words, the DCT coefficients give us an idea which frequencies reside in an image.

Secondly, the DCT coefficients are quantized according to a quantization table. The table, which is not specified by the standard, describes the correspondence between compression levels and quantization factors. Formally, the quantized value is calculated from the original one by dividing it by a quantization factor and rounding to the nearest integer. Quantization is an irreversible transformation leading to lossy data compression.

Thirdly, the quantized DCT coefficients are coded without loss of information applying Huffman coding.

Application of Benford features (first digits of the quantized DCT coefficients) is suggested in (Fu, 2007; Milani, 2014) for tampering detection in JPEG-compressed images. The hypothesis behind applying Benford features is that the naturally generated data follow Benford's law and the manipulated data violates it.

Benford's law states that the distribution of the first digits in a set of natural numbers is logarithmic. A set of numbers satisfies the generalized Benford law if the first digit x (x=1,2,…,9) occurs with a probability $p(x)$:

$$p(x) = n \cdot \log_{10}\left(1 + \frac{1}{\alpha + x^{\beta}}\right) \quad (1)$$

where n is the normalization factor and α, β are the parameters specifying the distribution.

Fu et al. (Fu, 2007) show that the quantized DCT coefficients of single-compressed JPEG images follow the generalized Benford law while the quantized DCT coefficients of double-compressed JPEG images violate it, which is reflected in the fact that the distribution of Benford features deviates from the logarithmic distribution.

Moreover, it is shown in (Milani, 2014) that the distribution of Benford features is specific for further levels of JPEG compression making the features a powerful instrument for revealing the image compression history.

Let Y_i denote the i-th quantized DCT coefficient, and N the number of DCT coefficients, then the first digits fd are computed as follows:

$$fd_i = \left\lfloor Y_i / 10^{\lfloor \log_{10} Y_i \rfloor} \right\rfloor \quad , \quad i = 1,2...,N \quad (2)$$

and the Benford features as follows:

$$Benf_j = \frac{1}{N}\sum_{i=1}^{N}\delta_i \quad , \quad \delta_i = \begin{cases} 1 & fd_i = j \\ 0 & fd_i \neq j \end{cases} \quad , \quad j = 1,2...,9 \quad (3)$$

4 OUR APPROACH TO GENERATION AND DETECTION OF MORPHS

4.1 Automatic Generation of Morphs

Our approach to automatic generation of face morphs follows the general morphing procedure described in Section 3.1. Aiming at creating a morph appearing similar to both persons, we generate only halfway morphs (α=0.5) where both images contribute equally. Hence, alpha-blending is nothing else but averaging. The mapping of triangles is done in the reverse way making use of bilinear interpolation. The discontinuities between triangles are concealed applying the 2x2 median filter.

There are 68 facial landmarks localized using the class `shape_predictor` from the dlib programming library (http://dlib.net/). Three landmarks depicting the lower contour of the upper lip are replaced by two landmarks at the lower lip. This adjustment is important because ID photographs require a closed mouth. Given that, the lower contour of the upper lip might overlap with the upper contour of the lower lip causing the triangles with collinear corners that are inappropriate for warping. Moreover, the set of landmarks is extended by two landmarks at the pupils and seven landmarks at the forehead (see Figure 1a).

(a) (b)

Figure 1: (a) Facial landmarks localized by dlib (green, blue), removed landmarks (blue) and our additional landmarks (red); (b) mask to apply smoothing filter.

Figure 2a depicts the generation of *complete morphs*. The workflow starts with extraction of facial landmarks which are extended by 20 landmarks on the image borders. Then the landmark coordinates are averaged. The blended landmarks are used for triangulation. The triangles from the first input image are warped to the average position resulting in the first warped image. Likewise, the second warped image is generated from the second input image. Finally, the warped images are averaged. Hence, a complete morph has mutual face geometry and texture. However, spurious shadows and strong visual inconsistencies in the hair region resulting from blending are the visual flaws that can hardly be concealed automatically. Therefore, we consider complete morphs to be inappropriate for the morphing attack, unless they have undergone a manual retouch.

Splicing Morphs are designed to overcome the visual flaws encountered in complete morphs. Figure 2b visualizes the morph generation process. After extracting facial landmarks, the convex hull representing a face is cut from the input images. The landmark coordinates are averaged and the blended landmarks are used for triangulation. The triangles from the first face are warped to the average position resulting in the first warped face. The same is done to obtain the second warped face. The warped faces are averaged in the frontal position similar to how is suggested in (Lee, 1998). This scheme allows for morphing three and more faces. The blended frontal face is warped back twice, namely to the face positions in the first and in the second input images. The result is two morphed faces. The final step is the splicing of the morphed faces into the corresponding original images. In order to make the transmission between the original and blended regions appear natural, all pixels in the mask in Figure 1b are smoothed by applying a Gaussian filter. The width of the mask and the parameters of the Gaussian filter are defined as relative values in accordance with the interpupillary distance.

The advantage of the proposed splicing approach is that a morph looks realistic because the seams of the blended region match the original face contour. The disadvantage is that, after inverse warping, the blended face has the same geometry as the face it is warped into. Therefore, the morph has a mutual texture, but the geometry is adopted from one of the input faces. Consequently, the splicing morphs are expected to match well with one subject. In order to match with another subject, both faces should have a similar geometry.

For perfectly frontal faces, inverse warping can be replaced by scaling and the blended face can be directly inserted into the one or other image. In this case, the blended face has an average geometry and an average texture, but the average geometry may differ from the original face geometry making seamless splicing extremely difficult.

Further factors impeding morphs from appearing realistic are different skin color and occlusion of face parts by hair e.g. abundant hair at the forehead region in input images. A straight-forward approach to control the quality of morphs is an automatic selection of input face images in regard to skin and hair. Analyzing and mitigating these factors will be a part of our future work.

The morph generation algorithm is implemented in Matlab.

4.2 Automatic Detection of Morphs

Based on the nine Benford features described in Section 3.2, we train the linear SVM classifier from two sets of images. The first one is comprised of splicing morphs and the second one encompasses original images as well as images after legitimate editing usually performed by photographers. This includes in-plane rotation, scaling and cropping. Notice that, after in-plane rotation, images are always cropped to get rid of blank corners.

The parameters for image editing operations are randomly chosen from the following ranges:

- cropping: from 60 to 80 pixels at every side (left, right, top, bottom);
- scaling factor: from 0.8 to 1.2;
- rotation angle: from -3° to 3°.

The set of “positive” samples contains 524 morphs that have been randomly selected from the whole set of 2614 splicing morphs. The set of “negative” samples contains 131 original, 131

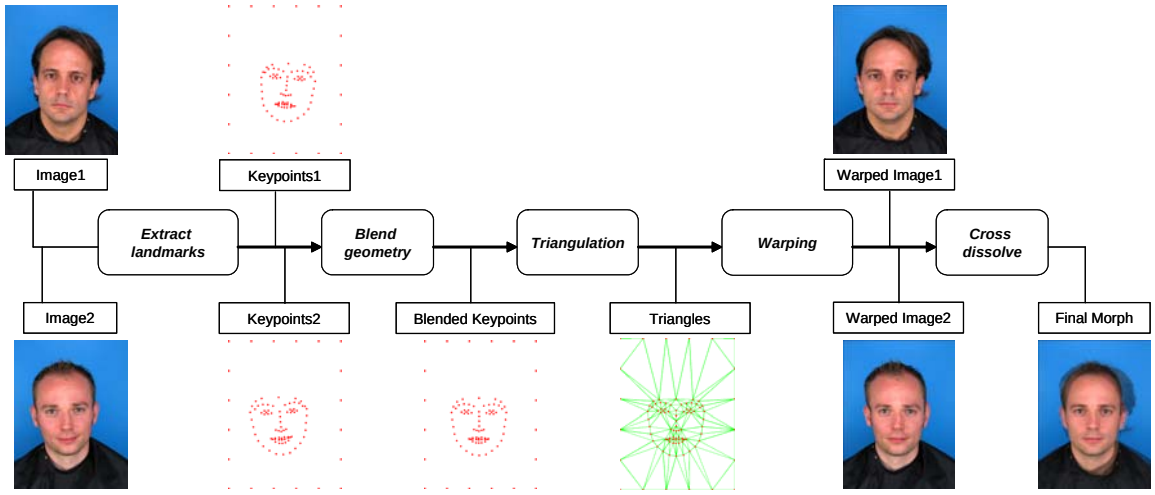

(a)

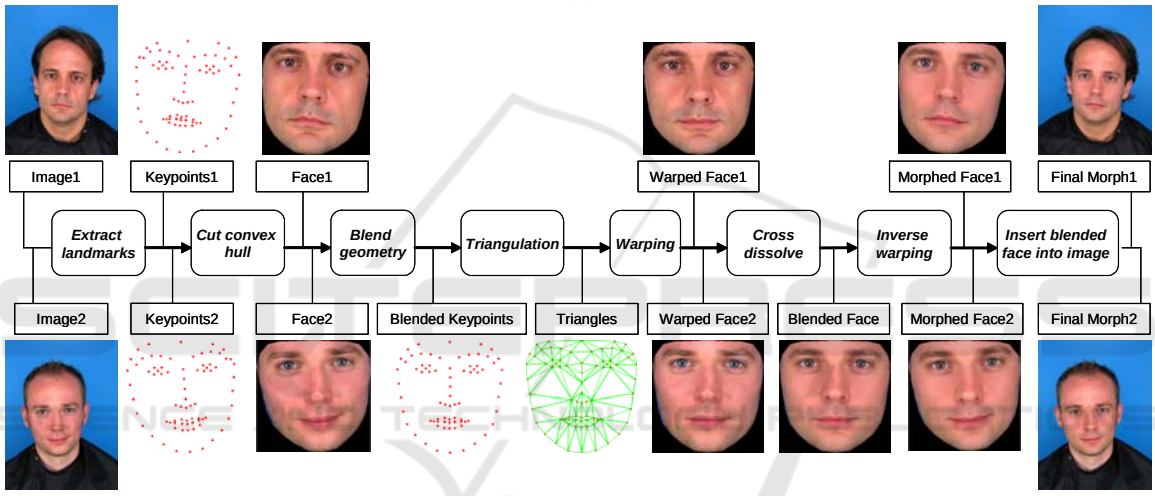

(b)

Figure 2: The workflow for the automatic generation of (a) complete morphs and (b) splicing morphs.

scaled, 131 cropped, and 131 rotated and cropped images, 524 samples in total. The equal number of positive and negative samples designates a balanced training set leading to the unbiased classifier. All training images are decompressed and then compressed in a JPEG format with 100% quality. For each test sample, the classifier makes a decision on which of two classes the sample belongs to. Before classification, all test images undergo re-compression similar to that which is done for training images. Training of the linear SVM classifier as well as classification of test samples is carried out with WEKA data mining software 3.8.0 (Hall, 2009) using default parameterization.

5 EXPERIMENTS

5.1 Evaluation Goals

The evaluation addresses the morph generation and morph detection approaches introduced in Sections 4.1 and 4.2 correspondingly. The quality of splicing morphs generated by the former is tested in two experiments on how well humans can recognize morphs as such (*Exp1*) and how many morphs would be accepted by a COTS AFR (*Exp2*). The classification performance of the latter is evaluated in the experiment (*Exp3*) with complete and splicing morphs from the Utrecht ECVP face dataset as well as with the original images and splicing morphs from the FEI Face Database.

5.2 Evaluation Dataset

The morphing attack is usually performed on ID photographs that are compliant with the ISO/IEC 19794-5 standard (ISO, 2011). In other words, a face pose in a photograph is frontal with the face parts located at particular regions. Facial expression is neutral and occlusions of eyes, nose or mouth do not occur. The interpupillary distance exceeds 120 pixels. Lighting is equally distributed on a face.

From among the publicly available face datasets, we have selected Utrecht ECVP face dataset as the one that best fits the ISO/IEC 19794-5 standard. It contains 131 images of 67 different individuals (20 women, 47 men). The image resolution yields 900x1200 pixels with the average interpupillary distance of 200 pixels. The majority of individuals are shot with neutral and smiling facial expressions.

Morphs are generated from all possible image pairs of 52 individuals (17 women, 35 men) utilizing only the images with neutral expressions. For each pair of images one complete morph and two splicing morphs are possible. Hence, 1326 complete morphs and 2614 splicing morphs were generated. Our algorithm failed to generate the remaining 38 splicing morphs because some triangles had collinear corners disabling warping. Finally, we manually selected 183 visually pleasing splicing morphs for evaluating human ability to distinguish between morphs and genuine images.

5.3 Performance Measures

In order to obtain uniform performance measures in all our experiments, we extend the standard performance measures of biometric systems expressed in terms of FAR/FRR by the MAR, which is used, on the one hand, for evaluation of AFR performance to reject morphs and, on the other hand, for humans and our morph detector to designate the relative number of morphs falsely classified as genuine images.

Assuming the matching score of an AFR system expresses the similarity between a probe and a gallery sample, the FAR is estimated by the relative number of impostor attempts with matching scores exceeding or equal to a decision threshold, while the FRR is estimated by the relative number of genuine attempts with matching scores lower than the threshold. Similarly, we estimate the MAR of an AFR system by the relative number of morph attempts with matching scores exceeding or equal to the threshold. Since a morph attempt is a special case of an impostor attempt, the MAR can be seen as a substitute for the FAR and the performance of an AFR system to reject morphs is expressed by the combination of MAR and FRR.

For biometric systems FAR and FRR are not equally important because the FAR is considered the security measure and the FRR the convenience measure. Therefore, the decision threshold is usually defined so that the FAR does not exceed a certain value and the FRR is then calculated at this threshold. Typical values for the FAR are 1% and 0.1%. It is common to denote the FRR at the decision threshold of 1% FAR as FRR_{100} and at the decision threshold of 0.1% FAR as FRR_{1000}. Following the same logic, MAR_{100} and MAR_{1000} are defined in (Ferrara, 2016).

The estimated MAR values give a pessimistic impression of the success of a morphing attack. Indeed, if a face image of person A is only slightly modified toward person B, an AFR system would still verify the morphed image against images of person A and would fail to verify the morphed image against images of person B. The MAR with such morphs would yield 50% implying that 50% of morph attempts have been falsely accepted. In reality, these morphs are useless because person B cannot use them to deceive an AFR system.

We propose to count the number of successful morphs instead of accepted morph attempts. A morph is successful if it has been verified against all gallery images of both persons. We call this performance measure the realistic MAR (rMAR).

For morph detection, no matter whether it is performed by humans or by an automated morph detection system, the "positive" decision is that an image is a morph and the "negative" decision is that an image is genuine. The MAR is, therefore, equal to the False Negative Rate (FNR) because a morph falsely accepted by an AFR system means a morph falsely missed by a morph detection system. The FRR is equal to the False Positive Rate (FPR), because a genuine image falsely rejected (as a morph) by an AFR system means a false alarm of a morph detection system. FNR and FPR completely describe detection performance. We also report the *classification accuracy* as the relative number of correct decisions in the total number of decisions. Since, for morph detection systems, each morph is associated with exactly one morphing attempt, the MAR equals the rMAR.

5.4 Evaluation of Morphs by Humans

The first experiment (*Exp1*) on the human capability to distinguish between morphs and genuine images

has two goals:

- evaluating the visual quality of our splicing morphs;
- obtaining clues on how humans recognize anomalies in portrait images to utilize this knowledge for developing algorithms for automatic morph detection.

For the experiment, we take 23 out of 183 pre-selected splicing morphs and 7 out of 15 genuine face images that have not been used for creating morphs. In total, there are 30 images in the test. The images are printed with standard photo quality on photo paper having the passport dimensions of 35x45 mm. Morphs and genuine photographs are mixed and presented sequentially to 42 participants under "thinking aloud test" conditions. Testees were asked to say whatever they think about the images and what pushes them to make one or another decision while performing morph detection.

The results are visualized in Figure 3. The classification accuracy of humans yields 55.62% with the MAR of 44.6% and the FRR of 43.64%. As can be seen in the diagram, 8 out of 23 morphs have been falsely recognized as genuine images by 50 and more percent of testees and only 3 morphs have been correctly detected by 70 and more percent of testees. Even worse is the situation with genuine images, 4 out of 7 genuine images have been falsely detected as morphs by 50 and more percent of testees.

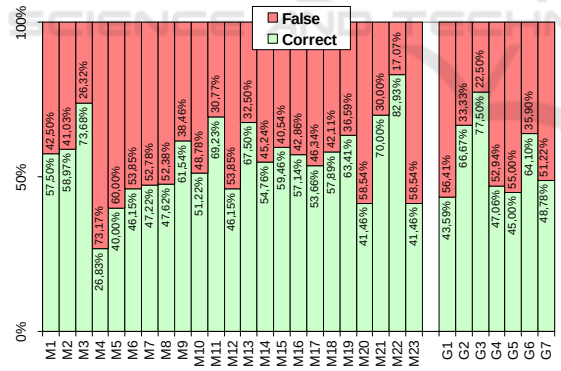

Figure 3: Results of the experiment on human capability to distinguish morphs (M1-23) from genuine images (G1-7).

Evaluating the morph detection performance of the testees separately, we see that the performance strongly fluctuates from one person to another. Only 9 out of 42 testees have correctly classified more than two thirds of test images. Six of them have mentioned blurring in the face region as a clue for indicating morphs and five of them also pointed to slight color differences in the face and the forehead regions.

All in all, this detection performance can be considered as close to random guessing enabling us to conclude that humans are not able to distinguish between splicing morphs and genuine images. This justifies the visual faultlessness of our automatically generated splicing morphs.

5.5 Evaluation of Morphs with the Reference AFR System

The second experiment (*Exp2*) aims at testing how many of our splicing morphs can deceive a COTS AFR system. Matching of face images is done with the Luxand FaceSDK 6.1 later referred to as "the matcher". The matcher produces similarity scores in the interval [0,1]. Based on the internal experiments, the SDK provides decision thresholds to obtain a given level of the FAR. The thresholds, at which the FAR yields 1% and 0.1%, are 0.99 and 0.999 correspondingly.

First, the matcher is evaluated with the complete Utrecht ECVP face dataset to get an idea about the distributions of genuine and impostor matching scores. 69 genuine scores result from the comparison of neutral and smiling faces (or two neutral faces) of the same person. 8446 impostor scores result from the pair-wise comparison of all images of different persons in the database. The distributions of genuine and impostor scores are depicted in Figure 4. All genuine scores are located in the interval [0.999, 1]. The mean value of the impostor scores yields 0.2645 while the maximum impostor score is 0.9751. In other words, the matcher shows the perfect result making no mistakes at both thresholds 0.99 and 0.999.

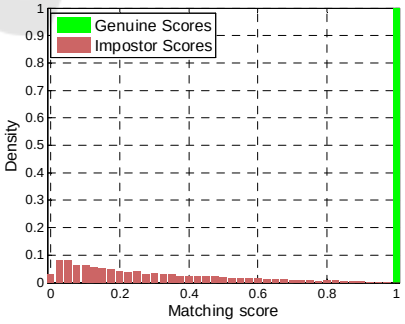

Figure 4: Distributions of genuine and impostor matching scores resulting from the cross-matching of original images in the Utrecht ECVP face dataset using the Luxand FaceSDK 6.1.

Second, 1326 complete and 2614 splicing morphs are matched against all images of the persons who participated in these particular morphs. Normally,

there are four morph attempts for each morphed image: two images with neutral faces (source images for morph generation) and two images with smiling faces. Notice that some persons do not have a smiling photograph and some persons have more than one neutral photograph. The distributions of matching scores for complete, splicing and manually selected splicing morphs are depicted in Figure 5. The corresponding values of MAR and rMAR are given in Table 1.

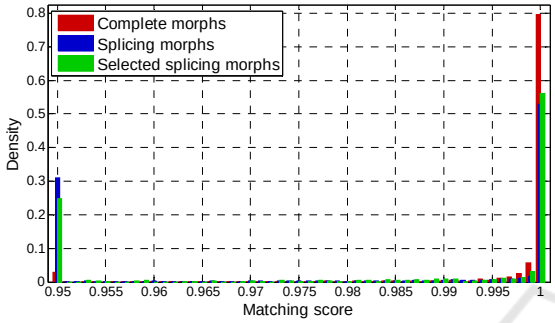

Figure 5: Distributions of matching scores resulting from matching of morphs against original images; the histogram bin yields 0.001; the left-most column shows the relative number of matching scores in the interval [0, 0.9501).

Despite their visual imperfection, most of the complete morphs are able to deceive the matcher. 83.27% of complete morph attempts are accepted at 0.1% FAR and 55.20% are verified against any of the genuine images in the test at the same threshold. The scores with splicing morphs are substantially lower. Only 53.77% of splicing morph attempts are accepted at 0.1% FAR and only 3.21% are verified against any of the genuine images. These 84 out of 2614 morphs (3.21%) can be considered perfect, having the characteristic that these would neither be detected by humans nor rejected by the reference AFR system.

Table 1: Pessimistic and realistic MAR at the decision thresholds of 1% and 0.1% of FAR.

	MAR_{100}	MAR_{1000}	$rMAR_{100}$	$rMAR_{1000}$
Complete morphs	93.34%	83.27%	80.39%	55.20%
Splicing morphs	60.59%	53.77%	11.78%	3.21%
Selected spl.morphs	65.43%	57.30%	16.94%	5.46%

In order to check whether the visually pleasing splicing morphs can better deceive the reference AFR, we have selected 183 out of 2614 and calculated MAR_{100} and MAR_{1000} for them. As can be seen in Table 1, the MAR values become slightly higher (see also Figure 5) but the difference in MAR values is still too low to assert that the realistic appearance of the face in a morphed image correlates with the performance of AFR to reject morphs.

5.6 Evaluation of Our Morph Detector

In the third experiment (*Exp3*), the performance of our morph detector is evaluated in two tests. In the first one, the 10-fold cross-validation is performed on the training dataset. In the second one, the morph detector is tested with four test datasets (T):

- T_1: the remaining 2090 splicing morphs from the Utrecht ECVP face dataset;
- T_2: 1326 complete morphs from the Utrecht ECVP face dataset;
- T_3: 400 original images from the FEI Face Database;
- T_4: 500 splicing morphs from the FEI Face Database.

The confusion matrix of the first test is depicted in Table 2. The classification accuracy yields 98.09% (1028/1048). Only 20 genuine images have been misclassified as morphs and none of the morphs has been misclassified as a genuine image.

Table 2: Confusion matrix of the 10-fold cross-validation of our morph detector.

Ground truth \ Classified as	Genuine	Splicing morphs
Genuine	**504 (96.18%)**	20 (3.82%)
Splicing morphs	0	**524 (100%)**

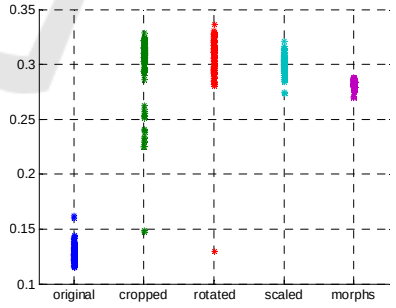

Figure 6: Distribution of samples for the feature $Benf_1$.

This result signifies that original and legitimately edited images have substantially different feature distribution compared to that of splicing morphs which is shown in the example of feature $Benf_1$ in Figure 6. The distribution of the feature values for splicing morphs is narrow with a small variation. The distributions of original and legitimately edited

images are broader with means significantly different from that of splicing morphs. Based on this diagram, we assert that the utilized features are not suitable to differentiate between the types of legitimate image editing but are highly suitable for distinguishing between splicing morphs and remaining images.

The results of the second test are depicted in Table 3. The MAR values of morphs created from Utrecht ECVP face dataset (T_1 and T_2) yield 12.11% for splicing morphs and 12.97% for complete morphs, indicating superior morph detection performance regarding humans. The classification accuracy of 98.44% (886/900) in the test with the FEI Face Database (T_3+T_4) indicates that the proposed classifier is capable of correctly classifying test images that are significantly different from images used for training.

Table 3: Classification results with four test datasets.

Classified as / Ground truth	Genuine	Morph
T_1 (morph)	253 (12.11%)	**1837 (87.89%)**
T_2 (morph)	172 (12.97%)	**1154 (87.03%)**
T_3 (genuine)	**386 (96.50%)**	14 (3.50%)
T_4 (morph)	0	**500 (100%)**

Nevertheless, the conducted test does not enable us to make conclusions about the general suitability of our proposed classifier. We realize that the distribution of Benford features can be different if morphs are generated from random face images using morphing techniques which are different from image warping with a subsequent cross-dissolve. Moreover, it is possible to create face images with the similar distributions of Benford features using legitimate image processing techniques. For instance, it is shown in (Wang, 2011) that the application of Benford's law to image tampering detection is vulnerable to the histogram manipulation attack.

6 CONCLUSIONS

In this paper, we have proposed (i) the approach to automatic generation of visually faultless facial morphs, (ii) the approach to morph detection by utilizing Benford features calculated from quantized DCT coefficients of JPEG-compressed images and (iii) evaluated both in three experiments.

The visual faultlessness of our splicing morphs is confirmed in the experiment with humans. The MAR of humans yields 44.60% with the FRR of 43.64% which is close to random guessing (see *Exp1*).

The suitability of our splicing morphs to deceive an AFR system has been tested in *Exp2*. Considering all verification attempts, the MAR_{100} is 60.59% and the MAR_{1000} is 53.77%. 11.78% of morphs have been verified against any of the genuine images at 1% FAR and 3.21% at 0.1% FAR.

Our morph detector yields 12.11% MAR with splicing and 12.97% MAR with complete morphs clearly outperforming humans. The classification accuracy of 98.44% with the alternative face database indicates that our morph detector is capable of correctly classifing test images that are fairly different from images used for training (see *Exp3*).

In our future work, we are going to visually improve morphs that will achieve higher matching scores with the reference AFR system. To this end, we plan an automatic selection of facial images with similar skin color, hair and head geometry along with automatic image editing including re-coloring and a hair retouch. We also plan engaging an alternative AFR system to the morph generation process for morph quality control by straight-away matching of just generated morphs against genuine images.

Our morph detector will be improved by considering the local features derived from blocks located at the face contour and in the face region. Following clues from the “thinking aloud test”, the local analysis of skin texture will be performed to detect excessive blurriness in the face region and color inconsistencies.

Due to the severity of the morphing attack and the limited capability of AFR systems to reject morphs, we believe that much attention should be paid to adoption of tampering detection approaches from digital image forensics to facial morphing, potentially making automatic morphing detection an indispensable component of AFR systems.

ACKNOWLEDGEMENTS

The work in this paper has been funded in part by the German Federal Ministry of Education and Science (BMBF) through the research programme under the contract no. FKZ: 13KIS0509K.

REFERENCES

Arad, N., et al., 1994. Image Warping by Radial Basis Functions: Applications to Facial Expressions. In

CVGIP:Graph Models Image Proc.56(2), pp. 161-172.
Beier, T., Neely, S., 1992. Feature-based image metamorphosis. In *Comp. Graphics. 26(2)*, pp. 35-42.
Bianchi, T., Piva, A., 2012. Image Forgery Localization via Block-Grained Analysis of JPEG Artifacts. In *IEEE Trans. on Information Forensics and Security 7(3)*, pp. 1003-1017.
Bitouk, D., et al., 2008. Face Swapping: Automatically Replacing Faces in Photographs, In *ACM Trans. on Graphics 27(3)*, 39.
Blanz V., Vetter, T., 1999. A morphable model for the synthesis of 3D faces. In *Proc. Conf. on Computer Graphics and Interactive Techniques*, pp. 187-194.
Celiktutan, O., et al., B., 2013. A comparative study of face landmarking techniques. In *EURASIP Journal on Image and Video Processing 2013 (1)*, 1.
Cootes, T.F., Taylor, C.J., 2000. Statistical Models of Appearance for Computer Vision. *Technical Report*, University of Manchester.
Dirik, A.E., Memon, N., 2009. Image tamper detection based on demosaicing artifacts. In *Proc. IEEE Int. Conf. on Image Processing*, pp. 1497-1500.
Farid, H., 2009. Image forgery detection. In *IEEE Signal Processing Magazine 26(2)*, pp.16-25.
Ferrara, M., Franco, A., Maltoni, D., 2014. The magic passport. In *Proc. IEEE Int. Joint Conf. on Biometrics*, Clearwater, Florida, pp. 1-7.
Ferrara, M., Franco, A., Maltoni, D., 2016. On the Effects of Image Alterations on Face Recognition Accuracy. In *Bourlai, T. (ed.) Face Recognition Across the Electromagnetic Spectrum*, Springer, pp. 195-222.
Ferrara, P., Bianchi, T., De Rosa, A., Piva, A., 2012. Image Forgery Localization via Fine-Grained Analysis of CFA Artifacts. In *IEEE Trans. on Information Forensics and Security 7(5)*, pp. 1566-1577.
Fridrich, J., 2009. Digital image forensic using sensor noise. In *IEEE Sig. Proc. Magazine 26(2)*, pp.26-37.
Fu, D., Shi, Y.Q., Su, W., 2007. A generalized Benford's law for JPEG coefficients and its applications in image forensics. In *Proc. SPIE EI 6505*, San Jose, CA.
Ghatol, N., et al., 2013. Image Morphing Detection by Locating Tampered Pixels with Demosaicing Algorithms, In *Int.J.of Computer App.66(8)*, pp.23-26.
Hall, M., et al., 2009. The WEKA data mining software: An update. In *SIGKDD Explorations 11(1)*, pp. 10-18.
ISO, 2011. ISO/IEC 19794-5:2011, Information technology - Biometric data interchange formats, Part 5: Face image data.
Lee, S., et al., 1996. Image Metamorphosis with Scattered Feature Constraints. In *IEEE Trans. on Visualization and Computer Graphics 2(4)*, pp 337-354.
Lee, S., Wolberg, G., Shin, S.Y., 1998. Polymorph: Morphing Among Multiple Images. In *IEEE Computer Graphics and Applications 18(1)*, pp. 58-71.
Liao, J., et al., 2014. Automating Image Morphing using Structural Similarity on a Halfway Domain. In *ACM Transactions on Graphics 33(5)*, 168.
Lukáš, J., Fridrich, J., 2003. Estimation of primary quantization matrix in double compressed JPEG images. In *Proc. Digital Forensics Research Conference (DFRWS'03)*.
Lyu, S., Pan, X., Zhang, X., 2014. Exposing Region Splicing Forgeries with Blind Local Noise Estimation. In *Journal of Computer Vision 110(2)*, pp. 202-221.
Mahdian, B., Saic, S., 2010. A bibliography on blind methods for identifying image forgery. In *Signal Processing: Image Communication 25*, pp. 389-399.
Milani, S., et al, 2014. Discriminating multiple JPEG compressions using first digit features. In *APSIPA Trans. on Signal and Inf. Processing 3(e19)*, pp. 1-10.
Piva, A., 2013. An Overview on Image Forensics., In *ISRN Signal Processing*, Article ID 496701, 22 p.
Ramachandra, R., Raja, K., Busch, C., 2016. Demystifying Magical Passport: A Robust Morphed Face Image Detection Scheme. In *Proc. IEEE Int. Conf. on Biometrics: Theory, Appl., and Systems*.
Schetinger, V., Iuliani, M., Piva, A., Oliveira, M. M., 2016. Digital Image Forensics vs. Image Composition: An Indirect Arms Race. In *CoRR abs/1601.03239*.
Vyas, J.P., Joshi, M.V., Raval., M.S., 2015. Automatic target image detection for morphing. In *Journal of Visual Comm. and Image Represent. 27*, pp. 28-43.
Wang, J., et al., 2009. Understanding Benford's law and its vulnerability in image forensics. In *Proc. IEEE Int. Conf. on Multimedia and Expo*, pp. 1568-1571.
Weng, Y., et al., 2013. Hair interpolation for portrait morphing, In *Comp.Graph. Forum 32(7)*, pp. 79-84.
Wolberg, G., 1998. Image morphing: a survey, In *Visual Computer 14(8)*, pp. 360-372.
Wolberg, G., 1990. *Digital Image Warping*, IEEE Computer Society Press, Los Alamitos CA.
Wu, J., 2011. Face Recognition Jammer using Image Morphing. *Tech.Rep. No. ECE-2011-03*, Boston Uni.
Zanella, V., Ramirez, G., Vargas, H., Rosas, L.V., 2009. Automatic Morphing of Face Images. Adaptive and Natural Computing Alg., *LNCS 5495*, pp 600-608.